APPLIED PHYSICS LETTERS 110, 023503 (2017)

Solid-state neutron detectors based on thickness scalable hexagonal boron nitride

K. Ahmed,[1,a)] R. Dahal,[1] A. Weltz,[2] James J.-Q. Lu,[1] Y. Danon,[2] and I. B. Bhat[1]
[1]*Department of Electrical, Computer, and Systems Engineering, Rensselaer Polytechnic Institute, Troy, New York 12180, USA*
[2]*Department of Mechanical, Aerospace and Nuclear Engineering, Rensselaer Polytechnic Institute, Troy, New York 12180, USA*

(Received 11 October 2016; accepted 29 December 2016; published online 10 January 2017)

This paper reports on the device processing and characterization of hexagonal boron nitride (hBN) based solid-state thermal neutron detectors, where hBN thickness varied from 2.5 to 15 μm. These natural hBN epilayers (with 19.9% ^{10}B) were grown by a low pressure chemical vapor deposition process. Complete dry processing was adopted for the fabrication of these metal-semiconductor-metal (MSM) configuration detectors. These detectors showed intrinsic thermal neutron detection efficiency values of 0.86%, 2.4%, 3.15%, and 4.71% for natural hBN thickness values of 2.5, 7.5, 10, and 15 μm, respectively. Measured efficiencies are very close ($\geq$92%) to the theoretical maximum efficiencies for corresponding hBN thickness values for these detectors. This clearly shows the hBN thickness scalability of these detectors. A 15 μm thick hBN based MSM detector is expected to yield an efficiency of 21.4% if enriched hBN (with $\sim$100% ^{10}B) is used instead of natural hBN. These results demonstrate that the fabrication of hBN thickness scalable highly efficient thermal neutron detectors is possible. *Published by AIP Publishing.* [http://dx.doi.org/10.1063/1.4973927]

High efficiency neutron detectors are essential for homeland security and nuclear safeguards, since neutrons are a very specific indicator of special nuclear materials (SNMs). Development of solid-state neutron detectors (SSNDs) represents an emerging area of research, because the existing highest efficiency ^{3}He gas based neutron detectors have drawbacks such as high cost, bulky nature, and high pressure and high bias voltage requirement.[1–3] SSNDs utilize high thermal neutron capture cross section (σ) values of neutron sensitive isotopes such as ^{10}B ($\sigma = 3840$ barns) and ^{6}Li ($\sigma = 940$ barns).[2] Most SSNDs are microstructured Si filled with ^{10}B or ^{6}Li and are of heterogeneous type with separate neutron conversion and charge collection regions.[3,4] ^{10}B has a natural abundance of $\sim$19.9%[2] and is a constituent element of hexagonal boron nitride (hBN). hBN is therefore an excellent material for homogeneous SSND fabrication, where both neutron conversion and charge collection can occur in this semiconductor. hBN has a large bandgap, E_G (5.5 eV–6 eV[5–7]), and larger threshold displacement energy, E_d, values (19.4 eV for B atoms and 23 eV for N atoms[8]) compared to Si (13 eV), GaAs (9.8 eV), and GaN (19 eV).[9] E_d, a measure of bond strength, is the energy required to displace an atom from its lattice position. Large E_d values of hBN make hBN SSNDs radiation hardened. hBN SSNDs are also relatively insensitive to gamma rays.[10] Neutron interaction probability (p) of an hBN layer (with thickness t) can be estimated from the equation, $p = 1 - e^{-\Sigma t}$, where Σ ($=\sigma$N) is the macroscopic cross section of ^{10}B, where N is the atomic number density of ^{10}B. The maximum theoretical intrinsic thermal neutron detection efficiency (η_{theory}) for an hBN device is equal to the corresponding p value. η_{theory} values of 50% and 80% require hBN thickness (with 100% ^{10}B) of 35 and 80 μm, respectively.

This work reports on the growth of thick hBN of thickness ranging from 2.5 to 15 μm using a chemical vapor deposition (CVD) process. These hBN films were used to fabricate SSNDs with a metal-semiconductor-metal (MSM) configuration. Charge transport in these devices is along a-axis, which represents the highest charge carrier mobility path in hBN.[11] Device capacitance (C_{dev}) and dark current (I_{dev}) of an hBN MSM SSND are orders of magnitude lower compared to microstructured Si based SSNDs.[3,4,12] Since lower values of C_{dev} and I_{dev} allow for scaling to larger device areas, hBN MSM SSNDs can be scaled to much larger detection area compared to microstructured Si based SSNDs.[3,4,12] MSM devices with 2.5 to 15 μm thick hBN yielded close ($\geq$92%) to theoretically expected detection efficiencies, demonstrating the hBN thickness scalability of these devices.

A low-pressure CVD system was employed for the epitaxial growth of hBN on sapphire substrates. SiC coated graphite susceptors were used, which were heated by an induction heating system. Precursors were triethylboron (TEB) and ammonia (NH_3) for B and N, respectively. High purity Hydrogen (H_2) was used as the carrier gas with a fixed flow of 2 SLM for the entire growth durations. 100 Torr was the chamber pressure. In order to reduce the large lattice mismatch between hBN and sapphire, a 10-minute low temperature (850 °C) sapphire nitridation step was introduced before the hBN growth.[6,12] The amorphous and thin nitridated layer works as a nucleation layer for hBN and effectively reduces the lattice mismatch mentioned earlier.[6,12] The hBN growth was performed at a temperature of 1350 °C. 2.5 μm and 15 μm thick hBN films exhibited broad (002) hBN peaks at 26.2° and 26°, respectively,[11,12] indicating slightly larger c-lattice constant compared to that of bulk hBN (6.66 Å[13]). The optical image of an 8 μm thick hBN film grown on a

a)Electronic mail: ahmedk2@rpi.edu

RIGHTSLINK

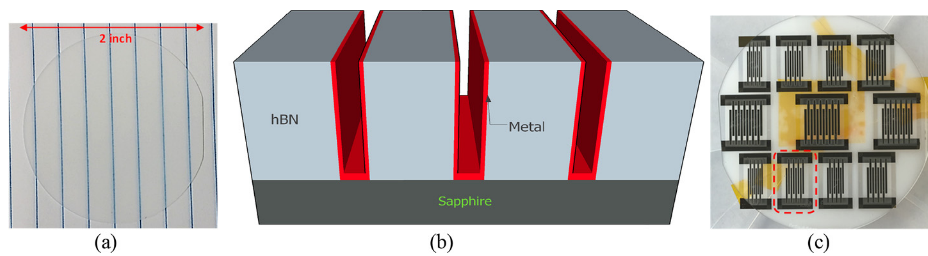

FIG. 1. (a) The optical image of an 8 μm hBN film on a 2-inch double side polished sapphire wafer (placed on a ruled paper), (b) schematic of an hBN MSM detector, and (c) the optical image of an array of detectors fabricated using a 15 μm thick hBN film. Detector D (with L = 250 μm and A = 14 mm^2) is the one highlighted by a red dashed rectangle. The yellow portion is the double sided Kapton tape at the backside of sapphire wafer used to attach it to a glass plate.

2-inch diameter double side polished sapphire wafer is illustrated in Fig. 1(a).

hBN SSNDs with an interdigitated electrode MSM architecture were fabricated with a complete dry processing technique developed at RPI. Figure 1(b) shows the schematic diagram of an hBN SSND. hBN films grown on sapphire substrates peel off the substrates as soon as they come in contact with any liquid if the film thickness is $>0.3\,\mu$m. Hence, wet processing (e.g., photolithography) was not an option for the fabrication of hBN MSM SSNDs. For the dry processing, stainless steel shadow masks were used for both hBN etching (to define the metal electrode areas) and metal deposition (to form the electrodes). hBN was completely etched in the electrode regions. hBN etching was done by inductively coupled plasma-reactive ion etching (ICP-RIE) using SF_6 plasma, and the etch rate was $\sim$0.8 μm/min. E-beam evaporation was used to deposit metal for electrode formation. Metal contacts were 30 nm Ni followed by 250 nm Ti. Four MSM devices were fabricated and characterized. The devices are: device A (t = 2.5 μm, electrode spacing, L = 1 mm, and area, A = 40 mm^2), device B (t = 7.5 μm, L = 250 μm, and A = 5 mm^2), device C (t = 10 μm, L = 200 μm, and A = 11.2 mm^2), and device D (t = 15 μm, L = 250 μm, and A = 14 mm^2). The optical image of device D is shown in Fig. 1(c).

hBN SSNDs (with t ranging from 2.5 to 15 μm) showed a strong response to deep UV light, as evidenced from the I-V characteristics of the detector D (with t = 15 μm) shown in Fig. 2(a). Undoped hBN epilayers showed the resistivity of $\sim 3 \times 10^9\ \Omega$ cm, which guarantees a very low dark current for the fabricated detectors. No persistent photoconductivity (PPC) effects are present in the detectors, as indicated by the photocurrent decay kinetics for the devices at a bias voltage, V = 150 V (not shown here). The responsivity as a function of wavelength (λ) for detector D is shown in Fig. 2(b). The detector, biased with 10 V, shows a peak responsivity wavelength (λ_P) of 215 nm and a cutoff wavelength (λ_C) of 225 nm, which correspond well with $E_G = 5.47$ eV measured for hBN films.[6] Responsivity decreases sharply for $\lambda > \lambda_C$, since these photons have insufficient energy to overcome bandgap energy. Below λ_P responsivity decreases gradually, since surface recombination loss increases from the reduced penetration depth.

A californium-252 (^{252}Cf) neutron source was used to measure neutron response of fabricated detectors. Since neutron capture cross section increases with the decreasing neutron energy, it is desirable to detect thermal neutrons (0.0259 eV) using these detectors. A high-density polyethylene (HDPE) block works as a moderator, which slows down fast neutrons (from ^{252}Cf source) and turns them into thermal neutrons. The neutron flux from the moderator includes both fast neutrons and thermal neutrons. Monte Carlo N-Particle Transport Code (MCNP) simulation was previously performed[3,14] to determine the energy distribution of the neutron flux, which matches a Maxwellian spectrum ($\varphi(E) \propto (E/KT)\exp(-E/KT)$ with KT = 0.034 eV. σ value for ^{10}B is 3450 barns at KT = 0.034 eV, whereas σ = 3840 barns at KT = 0.0259 eV. Σ values in this work are 35.01 cm^{-1} and 175.93 cm^{-1} for a natural hBN layer (with 19.9% ^{10}B) and an enriched hBN layer (with $\sim$100% ^{10}B), respectively. A comparison between the same MNCP calculations and experimentally measured neutron fluxes showed that overall neutron flux uncertainty is $<5\%$.[3] The detectors were enclosed in an Al box, which reduces the electronic noise by shielding the devices from external electromagnetic radiation. All the nuclear reaction pulse height spectra measurements were performed using the following electronics: an ORTEC 142PC charge sensitive preamplifier, an ORTEC

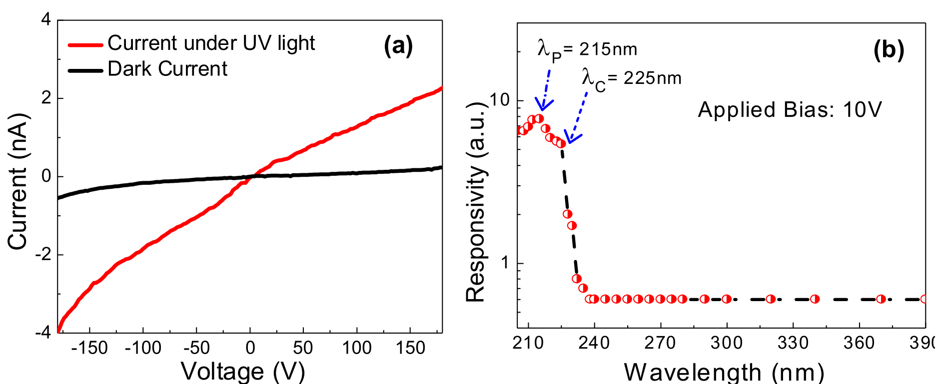

FIG. 2. (a) I-V characteristics and (b) spectral response of detector D. For this detector, t = 15 μm and L = 250 μm.

RIGHTSLINK

672 pulse shaping amplifier, and an ORTEC ASPEC-927 multichannel analyzer.

Carrier mobility-lifetime product ($\mu\tau$) is a crucial parameter for a neutron detector, since it determines the charge collection efficiency and hence the performance of the detector. Most of the electrons and holes generated by the nuclear reactions are collected by the electrodes under the applied electric field (E = V/L) if the recombination time (τ) of the free carriers is larger than the carrier transit time ($\tau_t = L/\mu E = L^2/\mu V$) in the material. Therefore, the $\mu\tau$ product should meet the requirement, $\mu\tau \geq L^2/V$ for a SSND.[11,15,16] Higher $\mu\tau$ products of the electrons and holes enable collection of the carriers at a smaller bias voltage for a given electrode spacing. To obtain the $\mu\tau$ product for the carriers, the photocurrent of device D (under UV illumination) was measured as a function of the applied voltage, which is shown in Fig. 3. Carrier excitation in hBN is uniform along the direction of electric field. For such a case, I–V characteristics are given by Many's equation,[17]

$$I(V) = I_0\left[\left\{\frac{\mu_n\tau_nV}{L^2}\left(1-\frac{\mu_n\tau_nV}{L^2}\left(1-e^{-\frac{L^2}{\mu_n\tau_nV}}\right)\right)\right\} + \left\{\frac{\mu_p\tau_pV}{L^2}\left(1-\frac{\mu_p\tau_pV}{L^2}\left(1-e^{-\frac{L^2}{\mu_p\tau_pV}}\right)\right)\right\}\right], \quad (1)$$

where $\mu_n\tau_n$ and $\mu_p\tau_p$ denote $\mu\tau$ products for electron and hole, respectively. I_0 is the saturation photocurrent. Both $\mu_n\tau_n$ and $\mu_p\tau_p$ values are obtained by fitting the measured I–V characteristics with the relation of Eq. (1). Fitted $\mu\tau$ values for this 15 μm hBN film (of detector D) are $\mu_n\tau_n = 3 \times 10^{-7}$ cm^2/V and $\mu_p\tau_p = 5 \times 10^{-8}$ cm^2/V.

Intrinsic thermal neutron detection efficiency (η) was measured for four different detectors (A, B, C, and D). For η measurement, the devices were placed 8 cm away from the front face of the moderator housing. The gold foil activation method was previously used to calibrate the thermal neutron flux (φ) at this position. Calculated φ values at this position were 380 n/cm^2 s, 320 n/cm^2 s, 300 n/cm^2 s, and 298 n/cm^2 s, respectively, for these devices at the time of the corresponding measurements. Applied bias voltages for the devices were 700 V, 450 V, 600 V, and 700 V, respectively. Three different measurements were taken to obtain η of each of the detectors. The first two measurements were done with the ^{252}Cf source kept inside the moderator housing. This moderated neutron source emits fast neutrons and gamma rays along with thermal neutrons. The second measurement had a 2-mm thick cadmium (Cd) sheet in between the bare device and the moderator. Cd absorbs the thermal neutrons and allows the fast neutrons and gamma rays to pass through it. The difference in the count rates ($C_{Bare} - C_{Cd}$) represents the count rates caused by the thermal neutrons, where C_{Bare} and C_{Cd} are the count rates from the first and the second measurements, respectively. The ^{252}Cf source was taken out of the moderator housing for the third measurement to determine the electronic noise level. The equation for measuring η is as follows:

$$\eta = \frac{C_{Bare} - C_{Cd}}{\varphi A}. \quad (2)$$

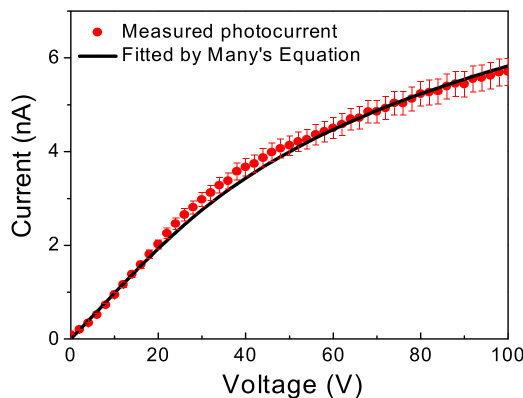

FIG. 3. I-V characteristics of detector D under UV illumination. Circles are the measured data, and the solid line is the fitted data using Eq. (1). Detector D has t = 15 μm and L = 250 μm. Error bars for the measured current are indicated in the plot.

The measured efficiency for the devices (A, B, C, and D) are 0.86 ± 0.03%, 2.4 ± 0.2%, 3.15 ± 0.12%, and 4.71 ± 0.18%, respectively. Figs. 4(a)–4(d) illustrate the associated pulse height spectra, respectively. η_{theory} values for these four natural hBN devices are 0.87%, 2.59%, 3.44%, and 5.11%, respectively. Effective neutron conversion efficiency ($\eta_{conv} = \eta/\eta_{theory}$) is termed as the fraction of the incident thermal neutrons that generated charge above the background noise level and therefore were counted by the detector. η_{conv} values for the devices are thus ≥92%. Natural TEB source (with 19.9% ^{10}B) was used for the hBN growth in this work. The enriched TEB source (with ∼100% ^{10}B) should not impact material properties of the hBN films, but increase the detection efficiency significantly. Considering the associated η_{conv} values, expected efficiencies for the four devices with enriched hBN films are 4.21%, 11.5%, 14.84%, and 21.37%, respectively. These results are summarized in Table I. Achievement of $\eta_{conv} \geq 92\%$ for SSNDs with t ranged from 2.5 to 15 μm illustrates the thickness scalability for these detectors. Fig. 4(e) demonstrates this thickness scaling phenomenon for hBN MSM SSNDs. If these results are extrapolated to a thicker (50 μm) hBN layer on sapphire with this type of MSM device structure, a natural hBN device (with 19.9% ^{10}B) should achieve an efficiency close to 20%, and an enriched hBN device (with ∼100% ^{10}B) should achieve an efficiency close to 60%. Further, low device capacitance (due to device geometry and the low dielectric constant of hBN) and low dark current (arising from high resistivity of hBN) ensure that these hBN SSNDs can be scaled up to much larger areas, as compared to microstructured Si based SSNDs.

In summary, CVD grown hBN films were used to fabricate neutron detectors with an MSM device structure. Developed detector fabrication process is a completely dry one involving shadow masks, which solves the typical problem of thick hBN films peeling off the sapphire substrate during wet processing. This process enabled MSM device fabrication with hBN films of thickness of up to 15 μm, with the possibility of even thicker hBN based device fabrication. hBN MSM devices, with thickness ranging from 2.5 to 15 μm, showed close (≥92%) to the corresponding theoretical maximum detection efficiencies, indicating the hBN

RIGHTSLINK

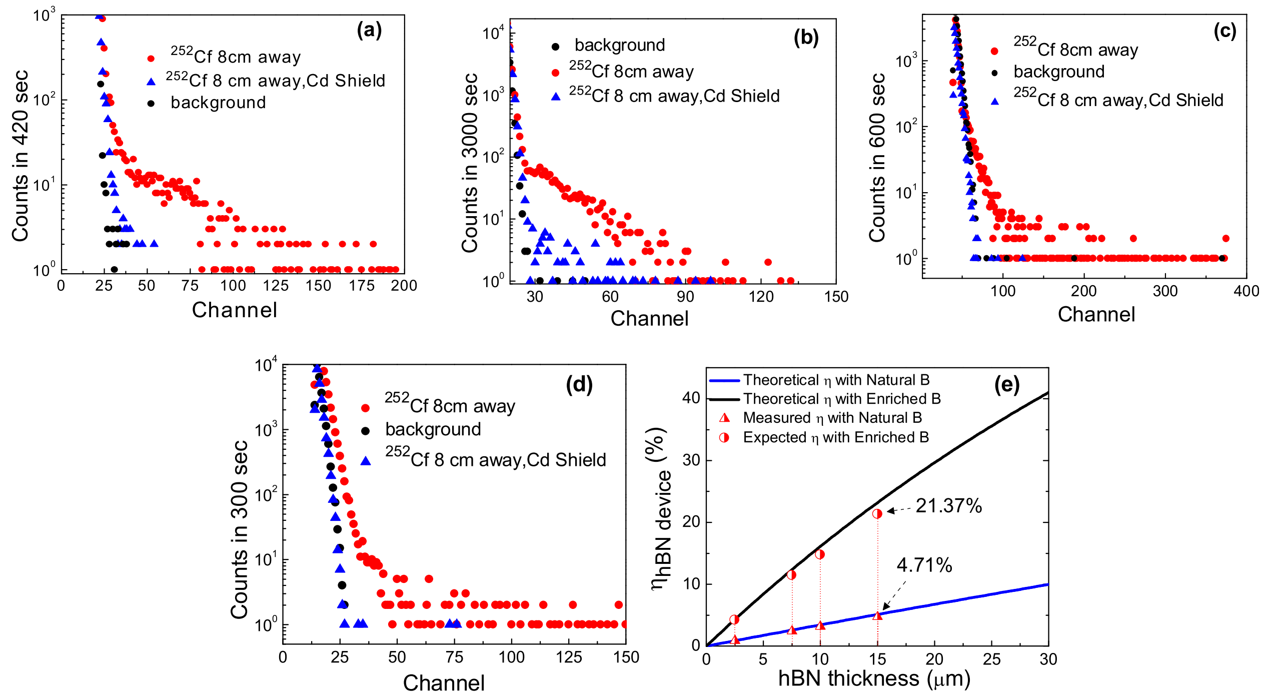

FIG. 4. Pulse height distribution of thermal neutrons measured with (a) detector A, (b) detector B, (c) detector C, and (d) detector D. (e) Theoretical and measured efficiency values of hBN detectors with different t values.

TABLE I. Efficiency values of SSNDs with hBN films of different thicknesses.

Device	hBN thickness (μm)	Measured η, natural hBN (%)	$\eta_{\rm theory}$, natural hBN (%)	$\eta_{\rm conv}$ (%)	Expected η, enriched hBN (%)	$\eta_{\rm theory}$, enriched hBN (%)
A	2.5	0.86	0.87	98	4.21	4.3
B	7.5	2.4	2.59	93	11.5	12.36
C	10	3.15	3.44	92	14.84	16.13
D	15	4.71	5.11	92	21.37	23.19

thickness scalability of these devices. Improvement in the material quality and the dry fabrication process and the usage of enriched TEB for hBN growth would further improve the performances of these detectors.

The authors acknowledge the support of the staff of the Rensselaer Polytechnic Institute Micro and Nano Fabrication Clean Room (RPI MNCR). This work was financially supported by the U.S. Department of Homeland Security, Domestic Nuclear Detection Office, under Grant Nos. ECCS-1348269 and 2013-DN-077-ER001.

[1]T. W. Crane and M. P. Baker, "Neutron Detectors," in *Passive Nondestructive Assay of Nuclear Materials*, edited by D. Reilly (Nuclear Regulatory Commission, NUREG/CR-5550, 1991).
[2]A. N. Caruso, J. Phys.: Condens. Matter **22**, 443201 (2010).
[3]K. C. Huang, R. Dahal, J.-Q. Lu, A. Weltz, Y. Danon, and I. Bhat, Nucl. Instrum. Methods Phys. Res. A **763**, 260 (2014).
[4]Q. Shao, L. F. Voss, A. M. Conway, R. J. Nikolic, M. A. Dar, and C. L. Cheung, Appl. Phys. Lett. **102**, 063505 (2013).
[5]K. Watanabe, T. Taniguchi, and H. Kanda, Nat. Mater. **3**, 404 (2004).
[6]K. Ahmed, R. Dahal, A. Weltz, J.-Q. Lu, Y. Danon, and I. Bhat, "Effects of sapphire nitridation and growth temperature on the epitaxial growth of hexagonal boron nitride on sapphire," pre-print arXiv:1609.00888 (2016).
[7]G. Cassabois, P. Valvin, and B. Gil, Nat. Photonics **10**, 262 (2016).
[8]J. Kotakoski, C. H. Jin, O. Lehtinen, K. Suenaga, and A. V. Krasheninnikov, Phys. Rev. B **82**, 113404 (2010).
[9]A. Ionascut-Nedelcescu, C. Carlone, A. Houdayer, H. J. von Bardeleben, J. L. Cantin, and S. Raymond, IEEE Trans. Nucl. Sci. **49**, 2733 (2002).
[10]K. Ahmed, R. Dahal, A. Weltz, J.-Q. Lu, Y. Danon, and I. Bhat, Appl. Phys. Lett. **109**, 113501 (2016).
[11]R. Dahal, K. Ahmed, J. W. Wu, A. Weltz, J.-Q. Lu, Y. Danon, and I. Bhat, Appl. Phys. Express **9**, 065801 (2016).
[12]K. Ahmed, R. Dahal, A. Weltz, J.-Q. Lu, Y. Danon, and I. Bhat, Vacuum **137**, 81 (2017).
[13]R. W. Lynch and H. G. J. Drickamer, J. Chem. Phys. **44**, 181 (1966).
[14]J. Clinton, "Optimization and characterization of a novel shelf powered solid state neutron detector," Ph.D. thesis (Rensselaer Polytechnic Institute, New York, USA, 2011).
[15]T. C. Doan, S. Majety, S. Grendadier, J. Li, J. Y. Lin, and H. X. Jiang, Nucl. Instrum. Methods Phys. Res., Sect. A **783**, 121 (2015).
[16]A. Maity, T. C. Doan, J. Li, J. Y. Lin, and H. X. Jiang, Appl. Phys. Lett. **109**, 072101 (2016).
[17]A. Many, J. Phys. Chem. Solids **26**, 575 (1965).

RIGHTSLINK